Complexes of a naphthalimide photoacid with organic bases, and their excited-state dynamics in polar aprotic organic solvents†

Tatu Kumpulainen,*‡ Bert H. Bakker, and Albert M. Brouwer*

Van 't Hoff Institute for Molecular Sciences, Faculty of Science, University of Amsterdam, PO Box 94157, 1090 GD Amsterdam The Netherlands

Email: tatu.kumpulainen@gmail.com, a.m.brouwer@uva.nl

‡ Present address: Physical Chemistry Department, Sciences II, University of Geneva, 30, Quai Ernest Ansermet, 1211 Geneva, Switzerland

Electronic Supplementary Information

Experimental Section

Synthesis and characterization of the compounds

Sodium 1,3-dioxo-1,3-dihydrobenzo[*de*]isochromene-5,8-disulfonate (S1) and **5,8-dihydroxybenzo[*de*]isochromene-1,3-dione (S2)** were synthesized by following the procedures reported in the literature.[1]

2-Butyl-5,8-dihydroxy-1*H*-benzo[*de*]isoquinoline-1,3(2*H*)-dione

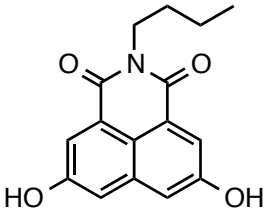

C_4-dHONI

A solution of 230 mg of **S2** and 1.0 ml of *n*-butylamine in 30 ml ethanol was refluxed under argon atmosphere for 20 h. The solution was concentrated under reduced pressure to give a solid residue. Purification by column chromatography over silica gel with ethyl acetate (R_f = 0.5) afforded 274 mg of pale yellow imide **C_4-dHONI** (96 %). Recrystallization from acetone/hexane gave 167 mg of crystals (needles) with mp. 310–311 °C.

^{1}H NMR (400 MHz, DMSO-d_6): δ (ppm) = 10.31 (s, 2H, OH), 7.79 (d, J = 2.3 Hz, 2H, naphthyl), 7.42 (d, J = 2.3 Hz, 2H, naphthyl), 3.99 (m, 2H, NCH_2), 1.58 (m, 2H, NCH_2CH_2), 1.34 (m, 2H, $NCH_2CH_2CH_2$), 0.92 (t, J = 7.4 Hz, CH_3); ^{13}C NMR (100 MHz; DMSO-d_6) (APT): δ (ppm) = 163.30 (CO, imide), 156.36 (COH), 135.40 (C, naphthyl), 123.22 (C, naphthyl), 118.70 (CH, naphthyl), 117.17 (C, naphthyl), 114.03 (CH, naphthyl), 39.40 (NCH_2), 29.64 (CH_2), 19.80 (CH_2), 13.71 (CH_3); IR (solid): $\tilde{\nu}$ (cm^{-1}) = 3401 (OH), 2962, 1697, 1680, 1650, 1621, 1610, 1588, 1462, 1402, 1337, 1264, 1241, 882, and 800. FAB-MS (mNBA matrix): observed m/z = 286.1074 $[M+H]^+$, calculated for $C_{16}H_{15}NO_4+H^+$: m/z = 286.1079.

Time-correlated single photon counting setup

Fluorescence decays of the samples were measured using the time-correlated single photon counting (TCSPC) method which has been described previously.[2] Briefly, the excitation wavelength of 360 or 460 nm was generated by frequency doubling of the output of a tunable Ti:sapphire laser (Chameleon Ultra, Coherent) and fluorescence was detected with a multichannel plate photomultiplier tube (R3809U-50, Hamamatsu) through a monochromator (M20, Carl Zeiss). The overall instrument response was found to be ~25 ps (fwhm) measured from a scatterer (colloidal silica, Ludox).

The fluorescence decays were fitted[3] to a sum of one to five exponential functions (Eq. S1 with n = 1…5), convolved with the measured instrument response function. Goodness of the fits was judged by the residuals and the χ^2 values. The global fits were achieved by fitting multiple decays simultaneously with global lifetimes ($\tau_{i,glob}$). The decay associated spectra (DAS) were constructed by plotting the pre-exponential factors ($\alpha_i(\lambda)$) of each component as a function of the wavelength. The areas of the

decays at each wavelength were normalized to the corrected steady-state emission intensities.

$$I(t,\lambda) = \sum_{i=1}^{n} \alpha_i(\lambda) e^{-\frac{t}{\tau_i}} \quad \text{(S1)}$$

Calculated proton affinities of the model compounds

The proton affinities were calculated as a negative enthalpy change ($-\Delta H_{298}$), i.e. the energy released, in the reaction between a proton and the bases:

$$B + H^+ \rightarrow BH^+ \qquad \text{(proton affinity).} \quad \text{(S2)}$$

In the above reaction, B is either the neutral base or the negatively charged conjugate base of the model photoacid (**HONI**$^-$). The enthalpy can be obtained from the electronic energy (E_{elec}, including nuclear repulsion) by including the nuclear vibrational energy and the effect of the temperature (RT).[4,5] The changes in electronic energy (including nuclear repulsion but no zero-point correction) and enthalpy were calculated according to the following equations:

$$\Delta E_{elec} = E_{elec}(\text{products}) - E_{elec}(\text{reactants}), \quad \text{(S3)}$$

$$\Delta H_{298} = H_{298}(\text{products}) - H_{298}(\text{reactants}), \quad \text{(S4)}$$

$$H = U(\text{electronic} + \text{nuclear}) + RT. \quad \text{(S5)}$$

In the above equations E is the total electronic energy without zero-point correction, H enthalpy, U total internal energy, R molar gas constant and T temperature in K. Calculated proton affinities and the literature values are listed in Table S1.

Table S1: Calculated $-\Delta E_{elec}$ values and proton affinities ($-\Delta H_{298}$) of the model compounds. All values are reported in kcal/mol and calculated with B3LYP/TZ2P level of theory

compound	solvent	$-\Delta E_{elec}$	$-\Delta H_{298}$
IM	MeCN	166.1	158.1
DBU	MeCN	179.1	170.5
HONI$^-$	MeCN	176.0	168.3
IM	gas phase	233.2 (231.7)[a]	224.9 (225.3)[b]
DBU	gas phase	260.8	251.8 (250.5)[c]
HONI$^-$	gas phase	336.9	328.7

[a]Value from ref. 4; [b]value from ref. 6; [c]value from ref. 7.

NMI, used in the experiments, has slightly higher proton affinity ($-\Delta H_{298}$ = 227.6 kcal/mol in gas phase)[4] than **IM** but is expected to behave similarly.

Optimized ground- and excited-state geometries of 1:1 dHONI---DBU complex

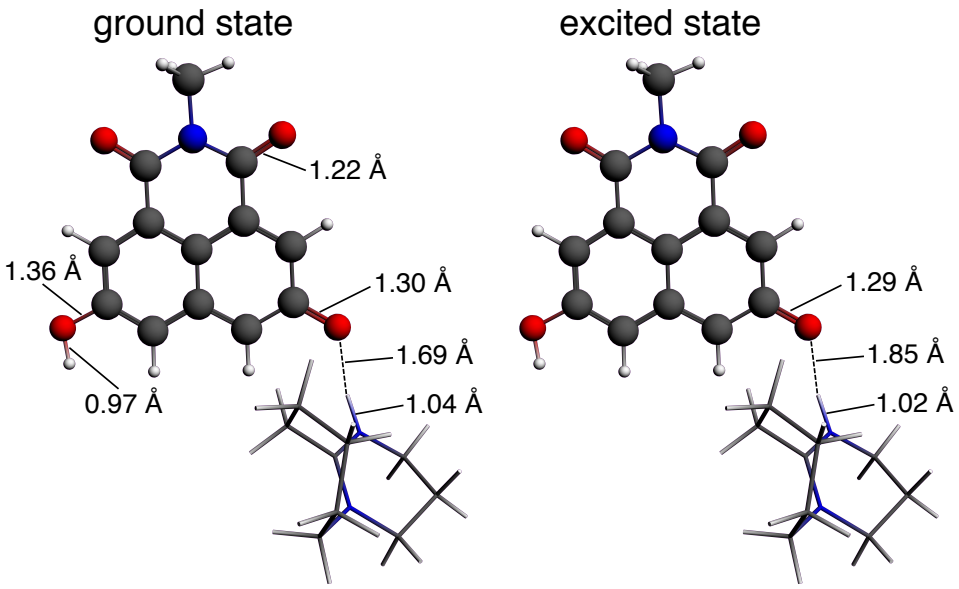

Fig. S1 Optimized ground- and excited-state geometries of **dHONI---DBU** complex in MeCN with relevant interatomic distances. Representative C=O, C−O and O−H distances are shown only for the ground-state geometry (left) and are not altered upon excitation.

Calculation of the radiative rate constants

The radiative rate constants were calculated with the Strickler-Berg relation:[8,9]

$$k_{\mathrm{f}} = 2.880 \times 10^{-9} n^2 (\tilde{\nu}_{\mathrm{em}}^3) \int_{S_1} \frac{\varepsilon(\nu)}{\nu} d\nu \,, \qquad \text{(S6)}$$

where $\varepsilon(\nu)$ is the molar absorption coefficient, n the solvent refractive index, and $\tilde{\nu}_{\mathrm{em}}^3$ a characteristic frequency of the emission spectrum, $F(\nu)$, defined by:

$$\tilde{\nu}_{\mathrm{em}}^3 = \frac{\int F(\nu) d\nu}{\int F(\nu) \nu^{-3} d\nu} \,. \qquad \text{(S7)}$$

The absorption spectra were integrated over the first absorption band (~310−430 nm) and scaled by a factor of 0.55. This is because the main absorption band consists of two transitions as demonstrated by the DFT calculations. Secondly, the comparison with the experimentally obtained values is easier after the scaling. The emission was integrated over the whole spectral range between 380−600 nm.

Derivation of the fitting functions for 1:2 association

The derivation of the fitting functions for 1:2 host(H)-guest(G) association is heavily adopted from the approach presented by Hargrove *et al.*[10] The two equilibrium reactions are:

$$H + G \rightleftharpoons HG, \tag{S8}$$

$$HG + G \rightleftharpoons HG_2, \tag{S9}$$

where the species involved are the host (H), the guest (G), the 1:1 complex (HG) and the 1:2 complex (HG_2). The association constants are defined as:

$$K_1 = \frac{[HG]}{[H][G]}, \tag{S10}$$

$$K_2 = \frac{[HG_2]}{[HG][G]}, \tag{S11}$$

where K_1 and K_2 are the association constants for the formations of 1:1 and 1:2 complexes, respectively, and [X] is the concentration of species X. The total concentration of each species, $[X]_0$, can be derived from the stoichiometry:

$$[H]_0 = [H] + [HG] + [HG_2], \tag{S12}$$

$$[G]_0 = [G] + [HG] + 2[HG_2]. \tag{S13}$$

Now the goal is to derive an equation dependent on only one unknown, which can be related to the spectral properties. We choose [G] following ref. 10. First, we derive expressions for [H], [HG], and [HG2] using Eqs. (S10, S11, S12).

$$[H] = \frac{[H]_0}{1 + K_1[G] + K_1K_2[G]^2} \tag{S14}$$

$$[HG] = \frac{K_1[G][H]_0}{1 + K_1[G] + K_1K_2[G]^2} \tag{S15}$$

$$[HG_2] = \frac{K_1K_2[G]^2[H]_0}{1 + K_1[G] + K_1K_2[G]^2} \tag{S16}$$

Substituting Eqs. (S15, S16) into Eq. (S13) yields Eq. (S17), in which the only unknown variables are [G], K_1, and K_2.

$$[G]_0 = [G] + \frac{K_1[G] + 2K_1K_2[G]^2}{1 + K_1[G] + K_1K_2[G]^2}[H]_0 \tag{S17}$$

Rearranging Eq. (S17) results in cubic equation for [G], which can be expressed as Eq. (S18):

$$a[G]^3 + b[G]^2 + c[G] + d = 0, \tag{S18}$$

where

$$a = K_1K_2\,, \tag{S19}$$

$$b = K_1 + 2K_1K_2[H]_0 - K_1K_2[G]_0\,, \tag{S20}$$

$$c = 1 + K_1[H]_0 - K_1[G]_0\,, \tag{S21}$$

$$d = -[G]_0\,. \tag{S22}$$

With an expression for one of the concentrations in hand, we need to derive a relationship between the absorption and the guest concentration, [G]. We start by expressing the total absorbance as a function of molar fractions, f, and assume that the free guest does not absorb at the monitoring wavelength (this can be experimentally achieved by selecting the monitoring wavelength higher than the guest absorption or by subtracting the guest concentration from the sample concentration, we use the latter).

$$A(\lambda) = A_{\mathrm{H}}(\lambda)f_{\mathrm{H}} + A_{\mathrm{HG}}(\lambda)f_{\mathrm{HG}} + A_{\mathrm{HG_2}}(\lambda)f_{\mathrm{HG_2}} \tag{S23}$$

Substituting f_X = [X]/[X]$_0$ = [X]/[H]$_0$ and Eqs. (S14, S15, S16) into Eq. (S23) we obtain the final expression, Eq. (S24), used in the non-linear least squares fitting.

$$A(\lambda) = \frac{A_{\mathrm{H}}(\lambda) + A_{\mathrm{HG}}(\lambda)K_1[\mathrm{G}] + A_{\mathrm{HG_2}}(\lambda)K_1K_2[\mathrm{G}]^2}{1 + K_1[\mathrm{G}] + K_1K_2[\mathrm{G}]^2} \tag{S24}$$

The fitting parameters are the absorptions of the host, $A_{\mathrm{H}}(\lambda)$, 1:1 complex, $A_{\mathrm{HG}}(\lambda)$, and 1:2 complex, $A_{\mathrm{HG_2}}(\lambda)$, corresponding to the total concentration of the host, [H]$_0$, and the association constants, K_1 and K_2. The total host and guest concentrations are obtained from the experimental conditions. An experimental titration curve is obtained by plotting the absorption as a function of the total guest concentration. The complete spectra of all the species can be obtained by fitting the absorption spectra over a broad wavelength range globally.

Instead of using the analytical expression for [G] in Eq. (S24), we will evaluate it numerically using Newton's method (also known as the Newton-Raphson method).[11] The true value of (x) i.e. the root of Eq. (S18) is approximated using an iterative method based on Eq. (S25).

$$x_{n+1} = x_n - \frac{f(x_n)}{f'(x_n)} \tag{S25}$$

In Eq. (S25), $f(x)$ is the left hand side of Eq. (S18) and $f'(x)$ is its first derivative. Since the root (x) corresponds to the x-intercept (y = 0), $f(x_n)$ approaches zero as the estimated values (x_n) become closer to the true solution. At the same time, the second right hand side term in Eq. (S25), often referred to as the step, becomes smaller. In the equation, an initial guess (n = 0) is used as an input to determine the first iteration value (x_1). In our case [G] = [G]$_0$ is used as the initial guess value. The first iteration value (x_1) is then used to determine the second (x_2) and process is repeated until (x_n+1) equals (x_n) i.e. $f(x_n) \approx 0$ and the real root of the equation is found.

With all the necessary equations in hand, the whole fitting process is as follows:

i) The initial guess values of the association constants and concentrations are used to numerically approximate the values of [G].
ii) The approximated values of [G] are then used in Eq. (S24) to do the non-linear least squares fitting to obtain new parameters.
iii) If the non-linear least squares analysis yields a sufficiently low value and the residual is good, the process is completed.
iv) If the fit is not good, the new parameters are used as new guess values and the process is started from the beginning.

The approach described above was implemented in MatLab 2012b to achieve global fits over a selected spectral range. The outputs of the program are the association constants, K_1 and K_2, and their 95 % confidence intervals, the spectra of all species, $A_H(\lambda)$, $A_{HG}(\lambda)$, and $A_{HG_2}(\lambda)$, concentration profiles of all species, and R^2 and χ^2 values to estimate the goodness of the fit.

Fitting functions for the 1:1 association model can be derived from above using K_2 = $[HG_2]$ = 0. This eventually results in an analytical fitting function, Eq. (S26), that can be used in the non-linear least squares fitting.

$$A(\lambda) = A_H(\lambda) + \frac{A_{HG}(\lambda) - A_H(\lambda)}{[H]_0}[G], \qquad \text{(S26)}$$

where

$$[G] = \frac{[G]_0 - [H]_0 - 1/K_1 + \sqrt{([G]_0 + [H]_0 + 1/K_1)^2 - 4[G]_0[H]_0}}{2}. \qquad \text{(S27)}$$

Additional spectra of C_4-dHONI

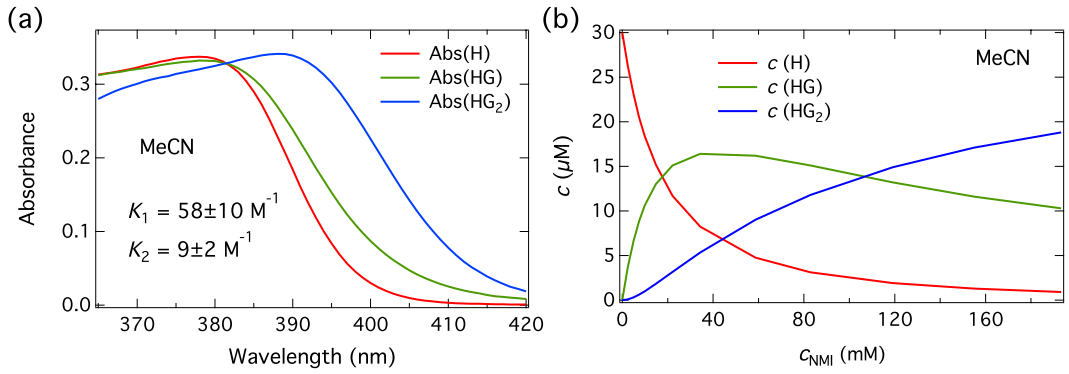

Fig. S2 (a) Fitted absorption spectra of all the species (H, HG, HG_2) at the total host concentration (c = 30 μM) and (b) the concentrations as a function of total **NMI** concentration in MeCN.

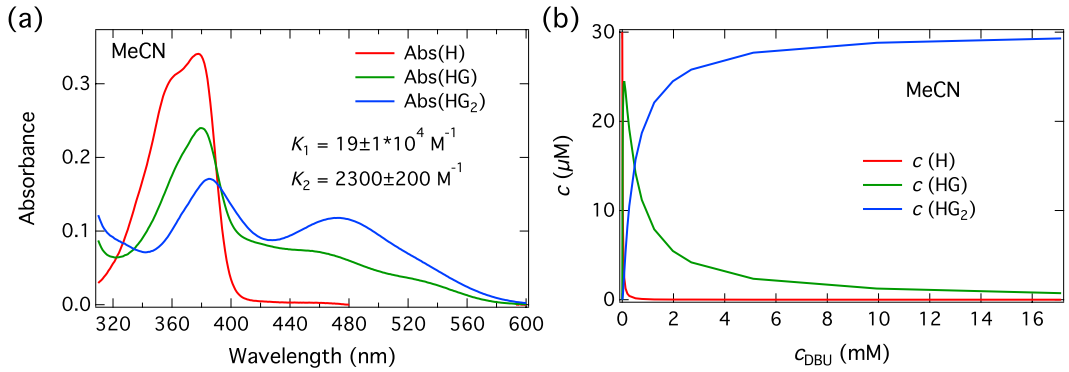

Fig. S3 (a) Fitted absorption spectra of all the species (H, HG, HG_2) at the total host concentration (c = 30 μM) and (b) the concentrations as a function of total **DBU** concentration in MeCN.

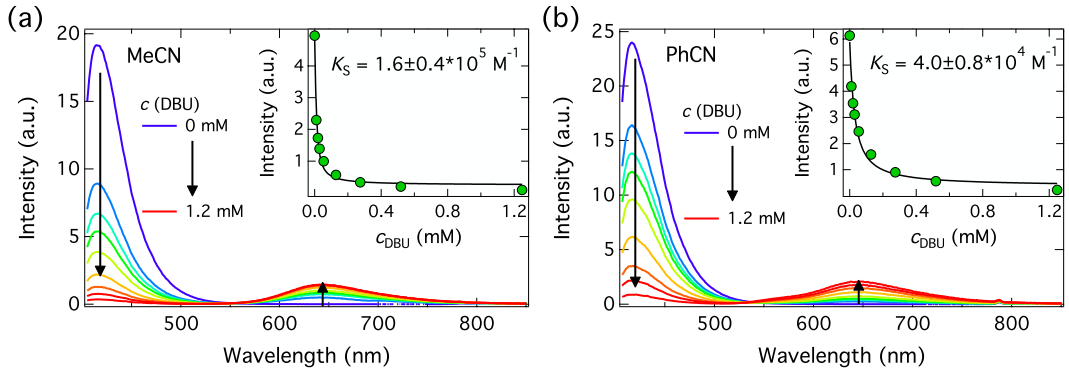

Fig. S4 Steady-state emission spectra of **C_4-dHONI** (c = 9 μM) upon addition of **DBU** in (a) MeCN and (b) PhCN. The excitation wavelengths were 390.5 nm and 392.5 nm in MeCN and PhCN, respectively. The insets show the integrated emission intensities together with fittings with the 1:1 association model. K_S is the static 1:1 quenching constant.

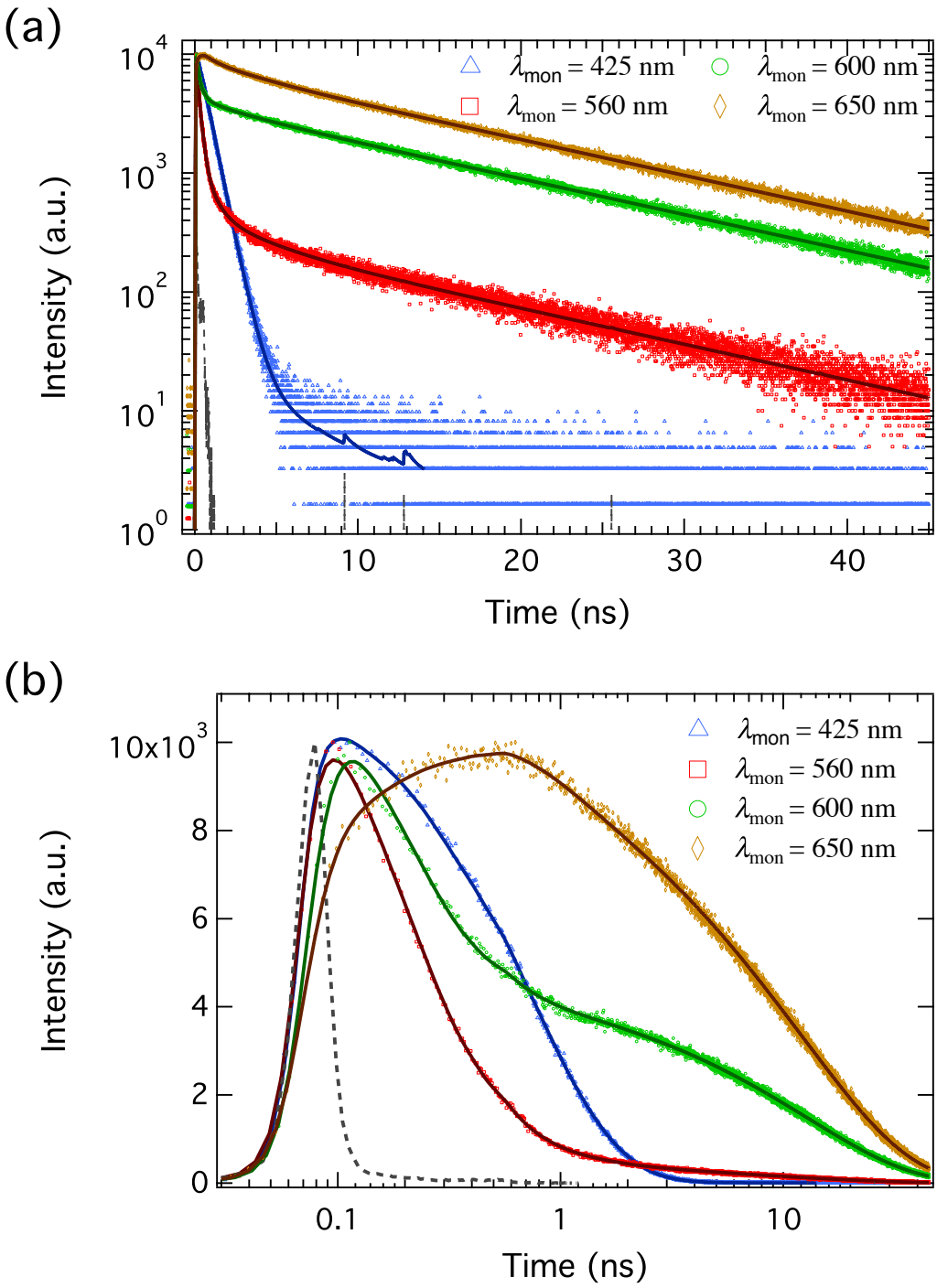

Fig. S5 Representative decay traces of **C_4-dHONI** (c = 40 μM) in MeCN in the presence of 200 mM of **NMI**. The excitation wavelength was 360 nm and monitoring wavelengths are indicated in the legends. Markers correspond to the data points and solid lines to the fittings with a five-exponential global model. The IRF is indicated by the dashed line. The traces in both figures are the same and are plotted on (a) log-lin and (b) lin-log scales to better show the different time scale components.

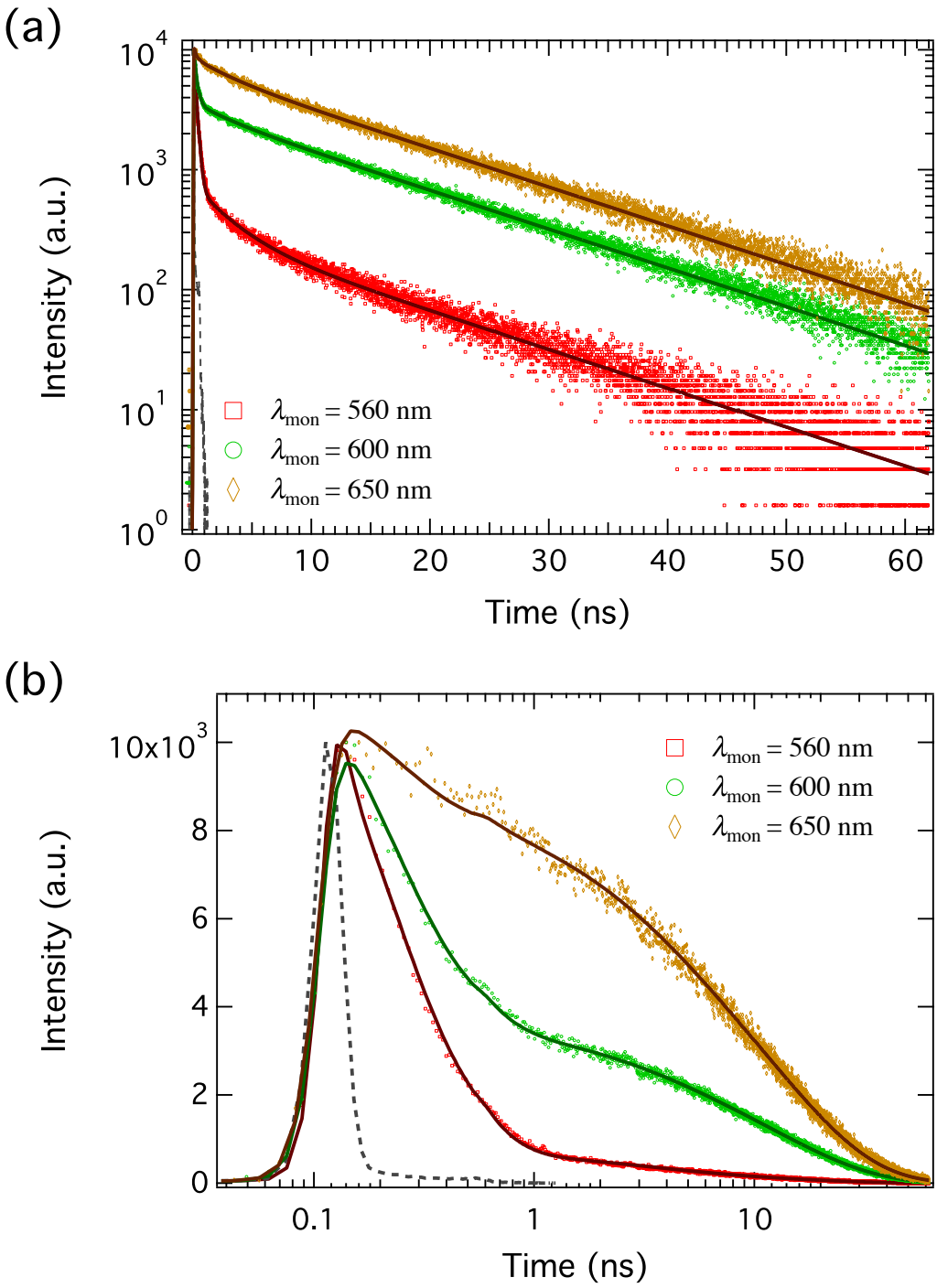

Fig. S6 Representative decay traces of **C_4-dHONI** (c = 40 μM) in MeCN in the presence of 250 μM of **DBU**. The excitation wavelength was 460 nm and monitoring wavelengths are indicated in the legends. Markers correspond to the data points and solid lines to the fittings with a three-exponential global model. The IRF is indicated by the dashed line. The traces in both figures are the same and are plotted on (a) log-lin and (b) lin-log scales to better show the different time scale components.

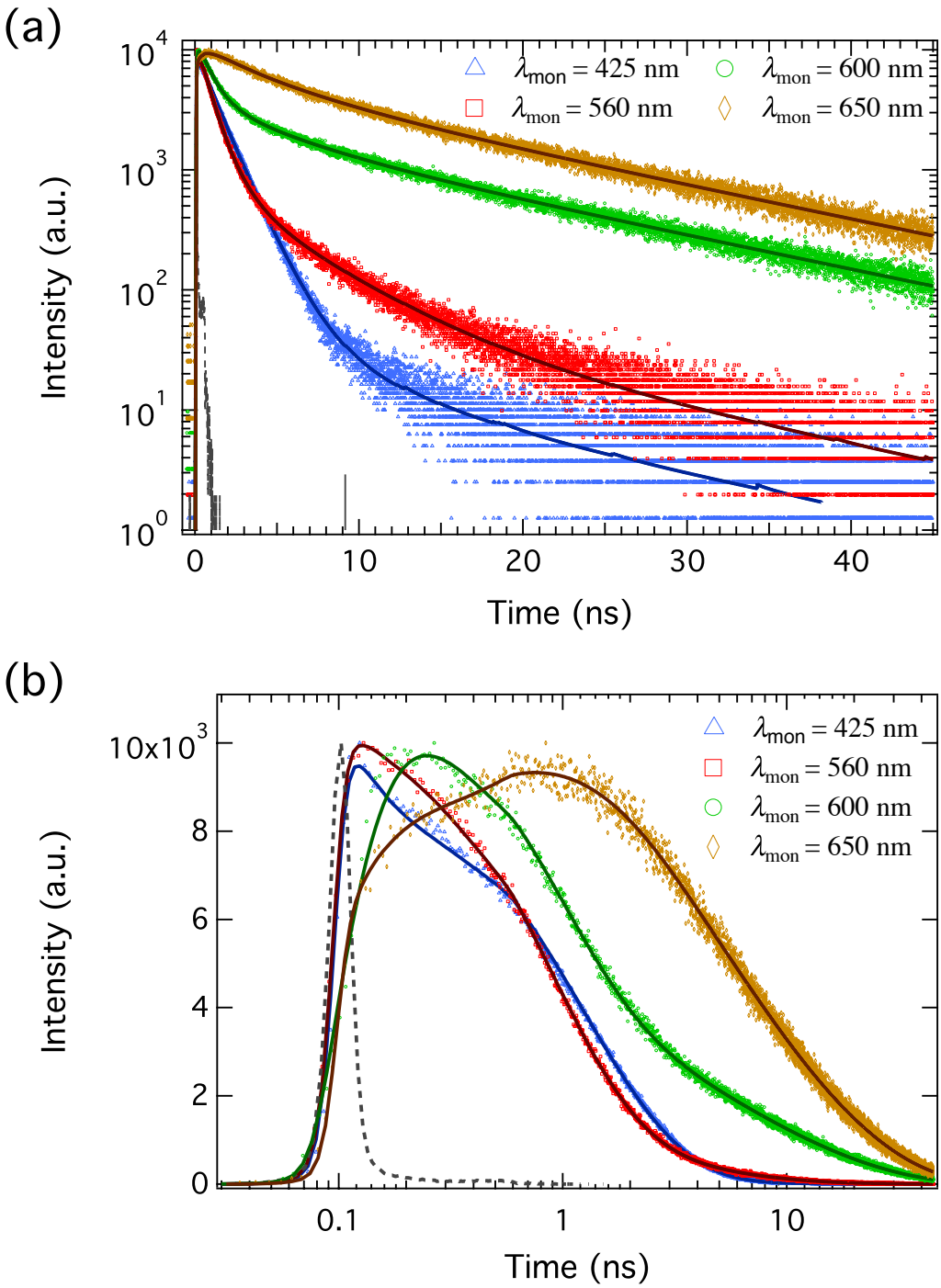

Fig. S7 Representative decay traces of **C_4-dHONI** (c = 40 μM) in PhCN in the presence of 200 mM of **NMI**. The excitation wavelength was 360 nm and monitoring wavelengths are indicated in the legends. Markers correspond to the data points and solid lines to the fittings with a five-exponential global model. The IRF is indicated by the dashed line. The traces in both figures are the same and are plotted on (a) log-lin and (b) lin-log scales to better show the different time scale components.

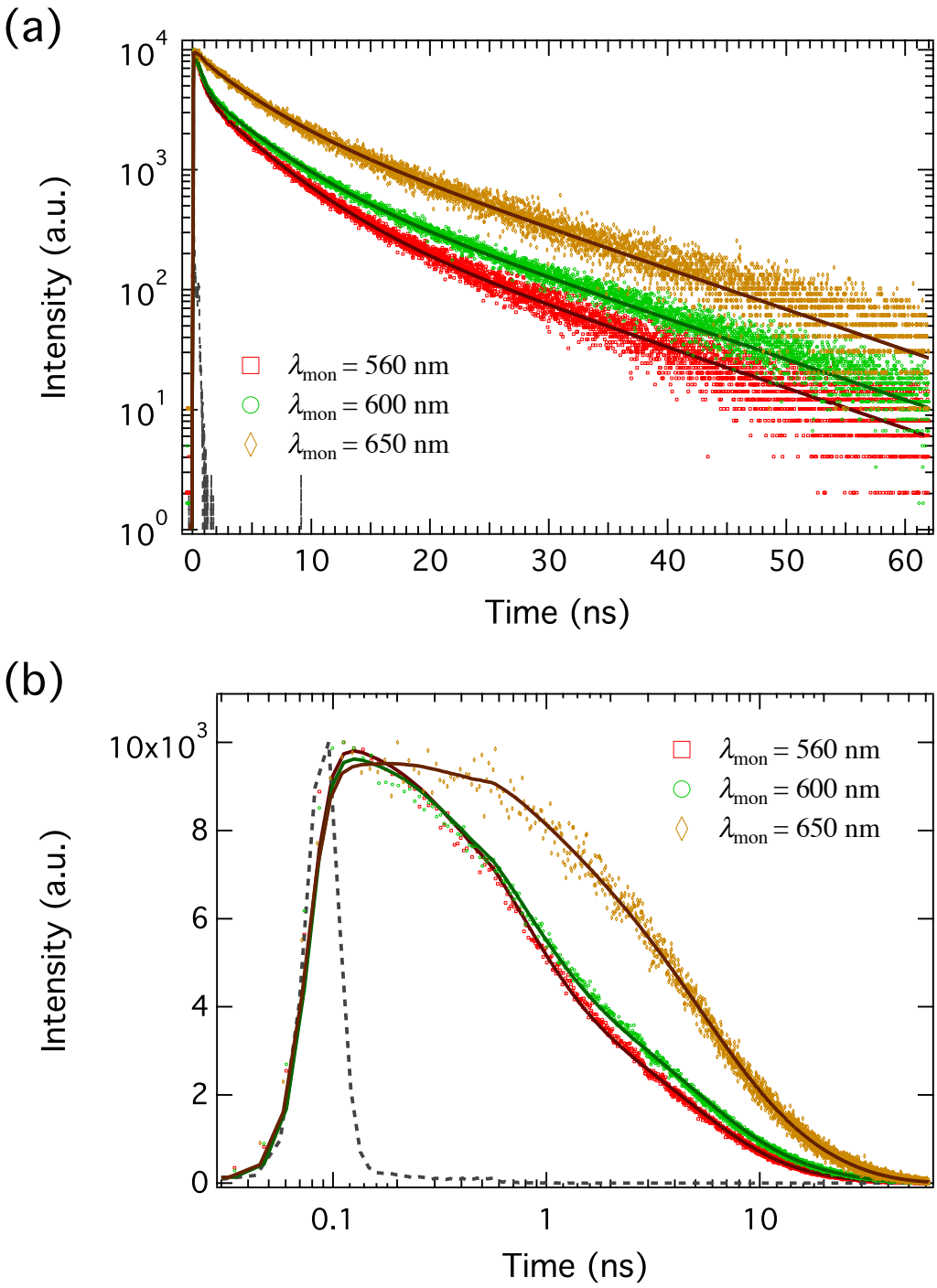

Fig. S8 Representative decay traces of **C_4-dHONI** (c = 40 μM) in PhCN in the presence of 250 μM of **DBU**. The excitation wavelength was 460 nm and monitoring wavelengths are indicated in the legends. Markers correspond to the data points and solid lines to the fittings with a three-exponential global model. The IRF is indicated by the dashed line. The traces in both figures are the same and are plotted on (a) log-lin and (b) lin-log scales to better show the different time scale components.

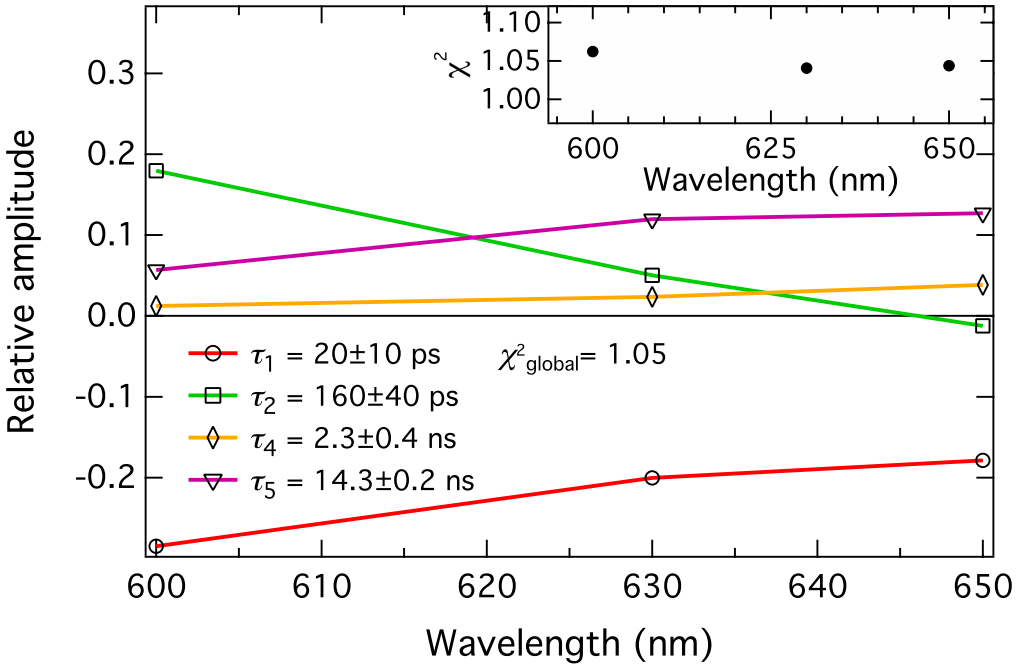

Fig. S9 Decay associated spectra (600–650 nm) of **C$_4$-dHONI** (c = 40 μM) in MeCN in the presence of 200 mM of **NMI**. The excitation wavelength was 360 nm. The inset shows the individual χ^2-values at each wavelength.

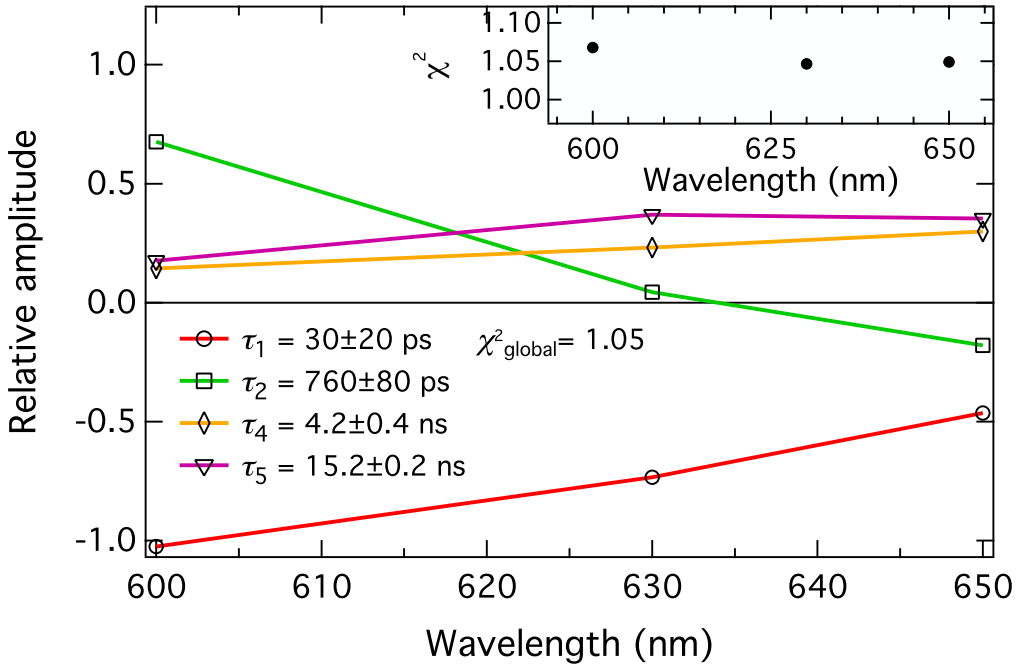

Fig. S10 Decay associated spectra (600–650 nm) of **C$_4$-dHONI** (c = 40 μM) in PhCN in the presence of 200 mM of **NMI**. The excitation wavelength was 360 nm. The inset shows the individual χ^2-values at each wavelength.

Table S2: Fitting parameters of the decomposition of the emission spectra of **C_4-dHONI** in the presence of **NMI** in MeCN and PhCN. The spectra were decomposed using a sum of four Gaussian functions in the wavenumber domain.

	C_4-dHONI + NMI in MeCN			
species	**ROH**	**HBIP**	**SSIP**	**FIP**
$\tilde{\nu}_{max}$ (cm^{-1})	23931	17719	15747	14577
λ_{max} (nm)	418	564	635	686
FWHM (cm^{-1})	2529	1281	1957	2692
relative area (%)	9	1	47	43
	C_4-dHONI + NMI in PhCN			
species	**ROH**	**HBIP**	**SSIP**	**FIP**
$\tilde{\nu}_{max}$ (cm^{-1})	23842	18054	15617	14074
λ_{max} (nm)	419	554	640	711
FWHM (cm^{-1})	1873	1953	2144	2300
relative area (%)	2	10	64	24

Notes and references:

1 K. Dziewoński, T. Majewicz and L. Schimmer, *Bull. Int. Acad. Pol. Sci. Lett., Cl. Sci. Math., Ser. A*, 1936, 43–55.

2 T. Kumpulainen and A. M. Brouwer, *Phys. Chem. Chem. Phys.*, 2012, **14**, 13019–13026.

3 Decay analyses were carried out using DecFit version 0.5.0, 2009 by Nikolai V. Tkachenko, TUT, Tampere, Finland. Distributed under terms of GNU/GPL license.

4 H. J. Singh and U. Mukherjee, *J. Mol. Model.*, 2011, **17**, 2687–2692.

5 B. Kovačević, Z. Glasovac and Z. B. Maksić, *J. Phys. Org. Chem.*, 2002, **15**, 765–774.

6 E. P. L. Hunter and S. G. Lias, *J. Phys. Chem. Ref. Data*, 1998, **27**, 413–656.

7 H. Chen, D. R. Justes and R. G. Cooks, *Org. Lett.*, 2005, **7**, 3949–3952.

8 S. J. Strickler and R. A. Berg, *J. Chem. Phys.*, 1962, **37**, 814–822.

9 D. Toptygin, *J. Fluoresc.*, 2003, **13**, 201–219.

10 A. E. Hargrove, Z. Zhong, J. L. Sessler and E. V. Anslyn, *New J. Chem.*, 2010, **34**, 348–354.

11 F. S. Acton, Ed., *Numerical Methods That Work*; Harper & Row: New York, USA, 1970.